membranes

MDPI

Article

Electrosynthesis of Electrochromic Polymer Membranes Based on 3,6-Di(2-thienyl)carbazole and Thiophene Derivatives

Chung-Wen Kuo [1], Jui-Cheng Chang [2,3], Jeng-Kuei Chang [4], Sheng-Wei Huang [1], Pei-Ying Lee [2] and Tzi-Yi Wu [2,*]

1 Department of Chemical and Materials Engineering, National Kaohsiung University of Science and Technology, Kaohsiung 80778, Taiwan; welly@nkust.edu.tw (C.-W.K.); bill4794@gmail.com (S.-W.H.)
2 Department of Chemical Engineering and Materials Engineering, National Yunlin University of Science and Technology, Yunlin 64002, Taiwan; d700215@gmail.com (J.-C.C.); leepeiying1018@gmail.com (P.-Y.L.)
3 Bachelor Program in Interdisciplinary Studies, National Yunlin University of Science and Technology, Yunlin 64002, Taiwan
4 Department of Materials Science and Engineering, National Chiao Tung University, No. 1001 University Road, Hsinchu 30010, Taiwan; jkchang@nctu.edu.tw
* Correspondence: wuty@gemail.yuntech.edu.tw; Tel.: +886-5-534-2601 (ext. 4626)

Abstract: Five carbazole-containing polymeric membranes (PDTC, P(DTC-*co*-BTP), P(DTC-*co*-BTP2), P(DTC-*co*-TF), and P(DTC-*co*-TF2)) were electrodeposited on transparent conductive electrodes. P(DTC-*co*-BTP2) shows a high ΔT (68.4%) at 855 nm. The multichromic properties of P(DTC-*co*-TF2) membrane range between dark yellow, yellowish-green, gunmetal gray, and dark gray in various reduced and oxidized states. Polymer-based organic electrochromic devices are assembled using 2,2′-bithiophene- and 2-(2-thienyl)furan-based copolymers as anodic membranes, and poly(3,4-ethylenedioxythiophene)-poly(styrene sulfonic acid) (PEDOT-PSS) as the cathodic membrane. P(DTC-*co*-TF)/PEDOT-PSS electrochromic device (ECD) displays a high transmittance change (ΔT%) (43.4%) at 627 nm as well as a rapid switching time (less than 0.6 s) from a colored to a bleached state. Moreover, P(DTC-*co*-TF2)/PEDOT-PSS ECD shows satisfactory optical memory (the transmittance change is less than 2.9% in the colored state) and high coloration efficiency (512.6 cm^2 C^{-1}) at 627 nm.

Keywords: electrochromic behavior; spectroelectrochemical property; transmittance; dual-type electrochromic device; cycling stability

Citation: Kuo, C.-W.; Chang, J.-C.; Chang, J.-K.; Huang, S.-W.; Lee, P.-Y.; Wu, T.-Y. Electrosynthesis of Electrochromic Polymer Membranes Based on 3,6-Di(2-thienyl)carbazole and Thiophene Derivatives. *Membranes* **2021**, *11*, 125. https://doi.org/membranes11020125

Academic Editors: Annarosa Gugliuzza and Giovanni Battista Appetecchi
Received: 8 January 2021
Accepted: 4 February 2021
Published: 9 February 2021

1. Introduction

Electrochromism refers to when electroactive species undergo a reversible change in optical absorption properties during the electrochemical oxidation/reduction process, and the species are electrochromic materials [1–3]. In the past 20 years, electrochromic materials and electrochemical membrane materials have been utilized in several fields such as for architectural windows, helmet visors, rearview mirrors, optical displays [4], fuel cells [5–7], and supercapacitors [8,9]. Electrochromic materials are generally classified into two categories: (a) inorganic complexes and transition metal oxides and (b) organic polymers and viologen derivatives [10]. Among these chromic materials, organic electrochromic polymers have gained extensive attention for promising applications in electrochromic electrodes owing to their short response time, facile color-tuning by chemical structures modification, low-power consumption, and good solution processability [11].

The most commonly used conjugated polymeric materials are polycarbazole [12,13], poly(3,4-ethylenedioxythiophene) (PEDOT) [14], polythiophene [15], polyfuran [16], polypyrrole [17], polyaniline [18], polytriphenylamine [19–21], and polyindole [22,23]. Polycarbazole and polytriphenylamine have been extensively applied for various electronic and optical devices owing to their high hole transporting mobility and good photoactive and electroactive performances [24]. Hsiao et al. published the electrochromic properties of carbazole-

and triphenylamine-based polymers (P(PhCz-2Cz) and P(TPA-2Cz)). P(TPA-2Cz) film was colorless, dark green, and brown in its neutral, semi-oxidized, and fully oxidized states. P(PhCz-2Cz) displayed satisfactory electrochromic switching with a ΔT_{max} up to 35% at 1052 nm [25]. Oral et al. reported the electrochromic properties of a dual-type ECD, which employed polystyrene functionalized carbazole (PS-Carb) as the anodically coloring polymer. The ΔT of PS-Carb/PEDOT ECD was 38% at 640 nm and the response time was 1.1 s [26]. Polythiophene is a potentially useful electrode material due to its desirable stability to environment and high conductivity [27]. However, the onset oxidation potential of thiophene is higher than 1.5 V [28]. PEDOT is a derivative of polythiophene which introduces alkoxyl substituent groups into a thiophene ring. The onset oxidation potential of PEDOT is lower than polythiophene. PEDOT is light sky-blue and deep blue in doped and reduced states, respectively. Accordingly, PEDOT is a cathodically coloring layer in electrochromic devices (ECDs). Polyfuran possesses some particular properties such as high fluorescence, a high HOMO energy level, and adequate solubility [29]. Polyfurans synthesized using furan, bifuran, and trifuran have different electrochemical activities, polyfuran prepared using trifuran has the highest electrochemical activity [30].

In the present report, a homopolymer (PDTC), two 2,2′-bithiophene (BTP)-based copolymers (P(DTC-*co*-BTP) and P(DTC-*co*-BTP2)), and two 2-(2-thienyl) furan (TF)-based copolymers (P(DTC-*co*-TF) and P(DTC-*co*-TF2)) with different DTC/BTP and DTC/TF feed molar ratios are synthesized electrochemically to explore their promising applications in electrochromic products. A 3,6-di(2-thienyl)carbazole unit reveals that because two thiophenes are linked by a carbazole, the strong hole-transporting carbazole group raises the HOMO energy level of PDTC. Therefore, PDTC shows a lower onset potential of oxidation than that of polythiophene. The conjugated chain length of 2,2′-bithiophene is longer than that of thiophene. The onset oxidation potential of 2,2′-bithiophene is lower than that of thiophene. Accordingly, 2,2′-bithiophene is incorporated to the polymer backbone and electrochromic properties of 2,2′-bithiophene-based polymers are characterizated in this study. Moreover, 2-(2-thienyl)furan combines the properties of furan and thiophene, while the conjugated chain length of 2-(2-thienyl)furan is longer than those of furan and thiophene. It is interesting to explore the difference of electrochromic behaviors for 2,2′-bithiophene- and 2-(2-thienyl)furan-based polymer membranes. The electrode membranes could be useful for identifying additional transport properties to be associated to the electrochromic behavior. Furthermore, five ECDs consisted of PDTC, P(DTC-*co*-BTP), P(DTC-*co*-BTP2), P(DTC-*co*-TF), or P(DTC-*co*-TF2) as the anodic membrane, and PEDOT-PSS as the cathodic membrane were built and their spectroelectrochemical behaviors, electrochromic switching kinetics, and redox stability were explored in detail.

2. Experimental

2.1. Materials

2,2′-bithiophene and 2-(2-thienyl)furan were purchased from Alfa Aesar and Sigma-Aldrich, respectively. 3,6-di(2-thienyl)carbazole (DTC) was synthesized according to previous procedures [31]. Electrolytes of ECDs were prepared using a mixture of poly(methyl methacrylate) (PMMA), propylene carbonate (PC), and $LiClO_4$. The weight ratio of PMMA, PC, and $LiClO_4$ is 33:53:14 [32].

2.2. Electrochemical Preparation of PDTC, P(DTC-co-BTP), P(DTC-co-BTP2), P(DTC-co-TF), P(DTC-co-TF2) Films

The electrosynthesis of PDTC, P(DTC-*co*-BTP), P(DTC-*co*-BTP2), P(DTC-*co*-TF), and P(DTC-*co*-TF2) membranes was implemented in a 0.2 M $LiClO_4$/acetonitrile (ACN) solution, and the feed species and feed ratio of species for anodic polymers were displayed in Table 1. The 3,6-di(2-thienyl)carbazole- and thiophene derivatives-based homopolymer and copolymers were prepared potentiostatically at 1.2 V (vs. Ag/AgCl).

Table 1. Feed species of anodic polymers.

Electrodes	Anodic Polymers	Feed Species of Anodic Polymers	Feed Molar Ratio of Anodic Polymers
(a)	PDTC	2 mM DTC	Neat PDTC
(b)	P(DTC-*co*-BTP)	2 mM DTC + 2 mM BTP	DTC:BTP = 1:1
(c)	P(DTC-*co*-BTP2)	2 mM DTC + 4 mM BTP	DTC:BTP = 1:2
(d)	P(DTC-*co*-TF)	2 mM DTC + 2 mM TF	DTC:TF = 1:1
(e)	P(DTC-*co*-TF2)	2 mM DTC + 4 mM TF	DTC:TF = 1:2

2.3. Assembly of Electrochromic Devices

Polymer ECDs were fabricated using PDTC, P(DTC-*co*-BTP), P(DTC-*co*-BTP2), P(DTC-*co*-TF), or P(DTC-*co*-TF2) film as the anodic electrochromic layer and PEDOT-PSS film as the cathodic electrochromic layer. The electrodeposited areas of polymer films were 1×1.5 cm^2. The ECDs were assembled by arranging the anodic and cathodic films to face each other, and they were separated using a PMMA/PC/$LiClO_4$ electrolyte.

2.4. Characterizations of Electrodes and Devices

The electrochemical properties of polymer films were characterized using a CHI627E electrochemical analyzer/workstation. The electrochemical experiments were operated using a three component cell. The working electrode, counter electrode, and reference electrode were an ITO coated glass plate, a platinum wire, and an Ag/AgCl electrode, respectively. The spectroelectrochemical experiments of polymer films and ECDs were measured using an electrochemical workstation and a JASCO V-630 UV-Visible spectrophotometer.

3. Results and Discussion

3.1. Electrochemical Characterization

Figure 1 displays the electrooxidation curves of 2 mM DTC, 2 mM BTP, and 2 mM TF in 0.2 M $LiClO_4$/ACN solution, indicating that the onset potentials (E_{onset}) of oxidation for DTC, BTP, and TF were 0.88, 1.22, and 1.19 V, respectively. DTC displayed lower E_{onset} than those of BTP and TF, implying the electron donating carbazole unit of DTC decreased the E_{onset} significantly. Moreover, E_{onset} of 2-(2-thienyl)furan is slightly lower than that of 2,2′-bithiophene.

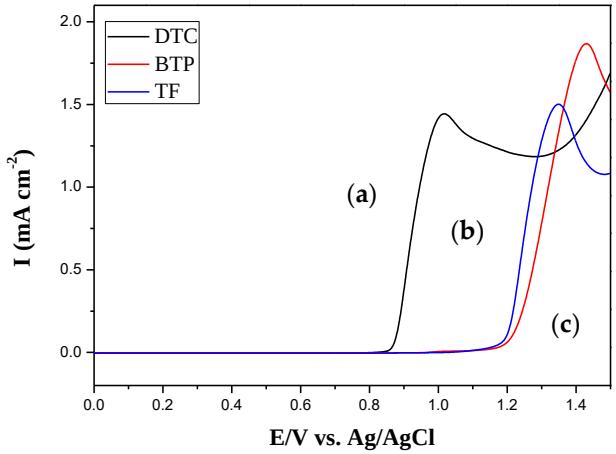

Figure 1. Electrooxidation curves of (**a**) 2 mM DTC, (**b**) 2 mM BTP, and (**c**) 2 mM TF in 0.2 M $LiClO_4$/acetonitrile (ACN) at a scan rate of 100 mV s^{-1}.

Figure 2 shows the electrosynthesized curves of PDTC, P(DTC-*co*-BTP), P(DTC-*co*-BTP2), P(DTC-*co*-TF), P(DTC-*co*-TF2), PBTP, and PTF in 0.2 M $LiClO_4$/ACN solution between 0.0 and 1.5 V. When the number of scanning curves increases, the peak current density increases with increasing number of cycles, indicating that the electrodeposition of

polymer membranes is present on ITO glasses [33]. The oxidized and reduced peaks of five polymer films were quasi-reversible. The oxidation peaks of PDTC, P(DTC-*co*-BTP), P(DTC-*co*-BTP2), P(DTC-*co*-TF), P(DTC-*co*-TF2), PBTP, and PTF films were located at ca. 1.27, 1.2, 1.25, 1.23, 1.26, 1.37, and 1.31 V (vs. Ag/AgCl), respectively. The reduction peaks of PDTC, P(DTC-*co*-BTP), P(DTC-*co*-BTP2), P(DTC-*co*-TF), P(DTC-*co*-TF2), PBTP, and PTF were situated at ca. 0.65, 0.48, 0.52, 0.43, 0.50, 0.63, and 0.60 V (vs. Ag/AgCl), respectively.

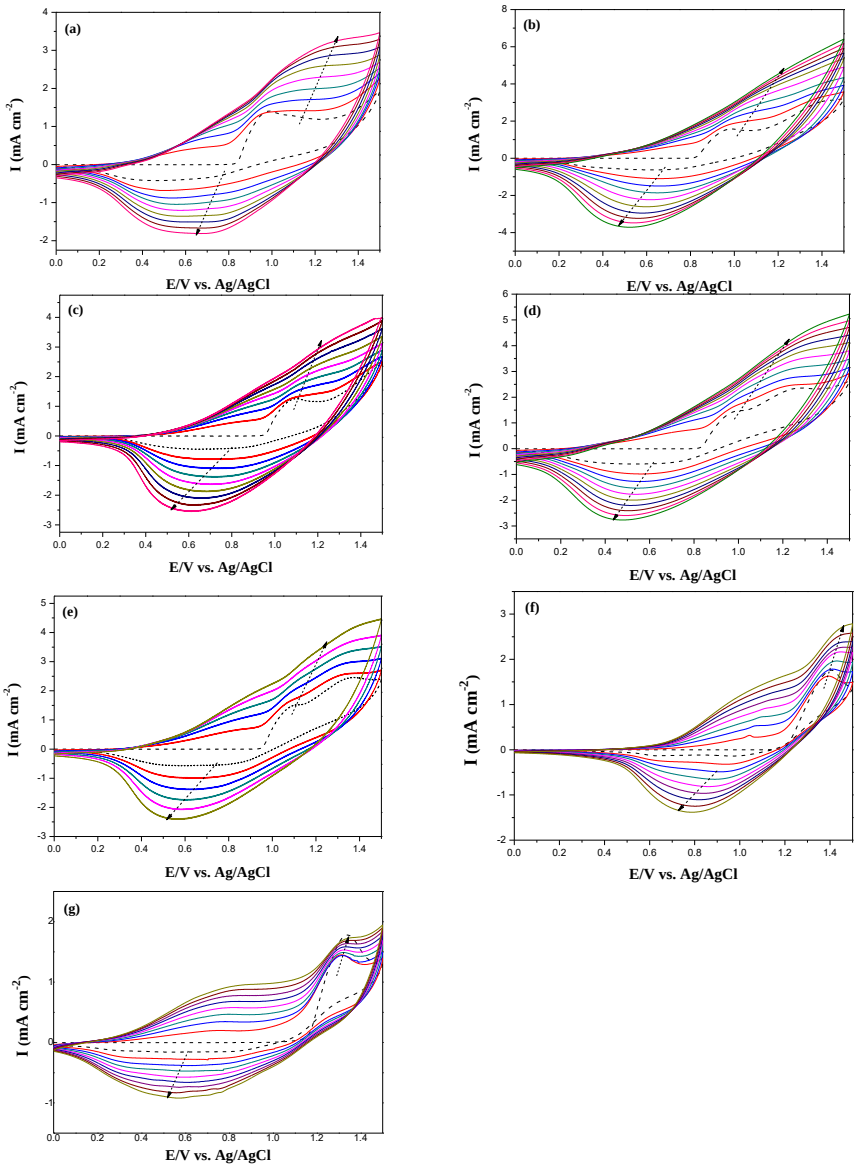

Figure 2. Electrochemical synthesis of (**a**) a homopolymer (PDTC), (**b**) P(DTC-*co*-BTP), (**c**) P(DTC-*co*-BTP2), (**d**) P(DTC-*co*-TF), (**e**) P(DTC-*co*-TF2), (**f**) PBTP, and (**g**) PTF in ACN solution at 100 mV s^{-1} on an ITO electrode.

The potentials and wave shapes of redox peaks of P(DTC-*co*-BTP), P(DTC-*co*-BTP2), P(DTC-*co*-TF), and P(DTC-*co*-TF2) are different to those of PDTC, PBTP, and PTF, proving the occurrence of copolymerization for P(DTC-*co*-BTP), P(DTC-*co*-BTP2), P(DTC-*co*-TF), and P(DTC-*co*-TF2) films. The general polymerization schemes of PDTC, P(DTC-*co*-BTP), and P(DTC-*co*-TF) are summarized in Figure 3. Specific capacitances of PDTC, P(DTC-*co*-BTP), P(DTC-*co*-BTP2), P(DTC-*co*-TF), and P(DTC-*co*-TF2) electrodes are 84, 109, 88, 98, and 92 F/g, respectively.

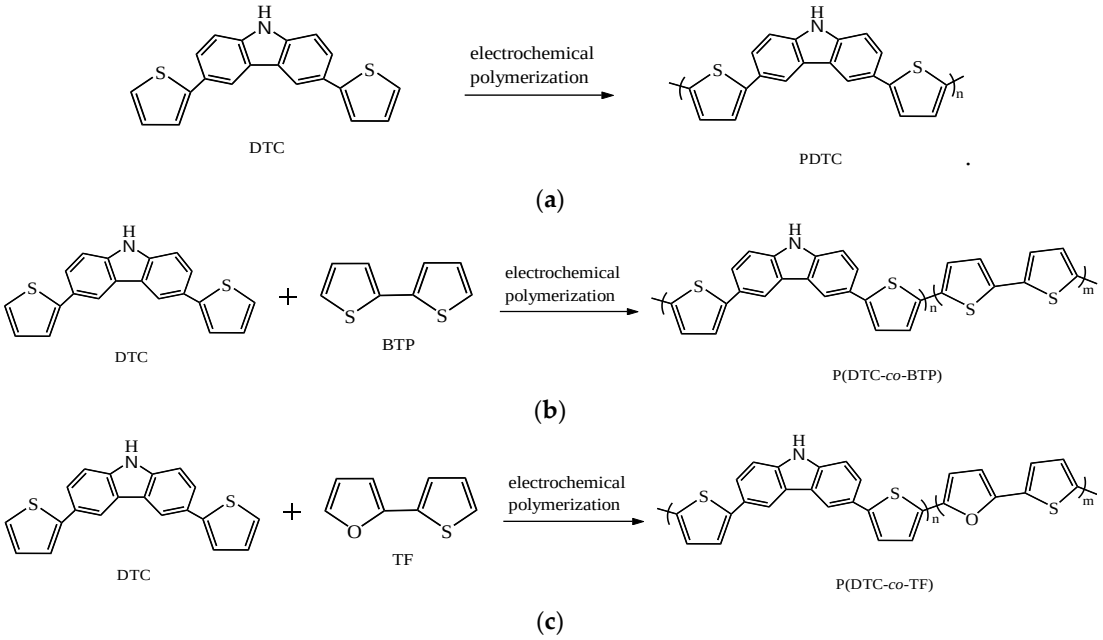

Figure 3. The electrochemical polymerization schemes of (**a**) PDTC, (**b**) P(DTC-*co*-BTP), and (**c**) P(DTC-*co*-TF).

Figure 4 shows the CV curves of PDTC, P(DTC-*co*-BTP), P(DTC-*co*-BTP2), P(DTC-*co*-TF), and P(DTC-*co*-TF2) films at scan rates of 10, 50, 100, 150, and 200 mV s^{-1} in 0.2 M $LiClO_4$/ACN. The anodic and cathodic peaks of PDTC, P(DTC-*co*-BTP), P(DTC-*co*-BTP2), P(DTC-*co*-TF), and P(DTC-*co*-TF2) membranes displayed *quasi*-reversible behaviors and the inset in Figure 4 revealed that the redox peak current density increased with the increasing scan rate linearly, demonstrating that the oxidation and reduction *processes* of PDTC, P(DTC-*co*-BTP), P(DTC-*co*-BTP2), P(DTC-*co*-TF), and P(DTC-*co*-TF2) films were not *diffusion*-limited [34].

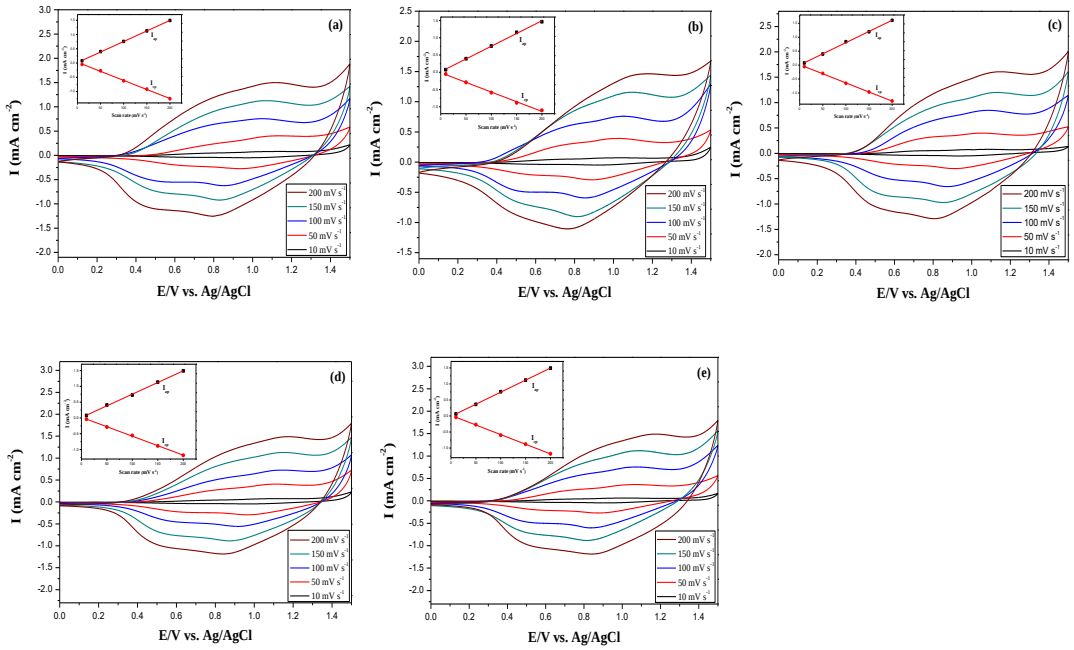

Figure 4. Cyclic voltammetry (CV) curves of (**a**) PDTC, (**b**) P(DTC-*co*-BTP), (**c**) P(DTC-*co*-BTP2), (**d**) P(DTC-*co*-TF), and (**e**) P(DTC-*co*-TF2) films at different scan rates between 10 and 200 mV s^{-1} in the $LiClO_4$ + ACN solution. Inset: Plots of scan rate vs. anodic and cathodic peak current densities.

3.2. Spectroelectrochemical Measurement of Polymers

Figure 5 displays absorption spectra of PDTC, P(DTC-*co*-BTP), P(DTC-*co*-BTP2), P(DTC-*co*-TF), and P(DTC-*co*-TF2) films in 0.2 M $LiClO_4$/ACN. At 0.0 and 0.2 V, PDTC, P(DTC-*co*-BTP), P(DTC-*co*-BTP2), P(DTC-*co*-TF), and P(DTC-*co*-TF2) films display definite-transition bands at ca. 400 nm. After increasing the applied voltage gradually, new charge carrier bands appeared at a long wavelength region. The charge carrier bands of PDTC were located at 550 nm and 860 nm. For the corresponding copolymers, the latter charge carrier bands of P(DTC-*co*-BTP), P(DTC-*co*-BTP2), P(DTC-*co*-TF), and P(DTC-*co*-TF2) were situated at 875, 855, 870, and 855 nm, respectively.

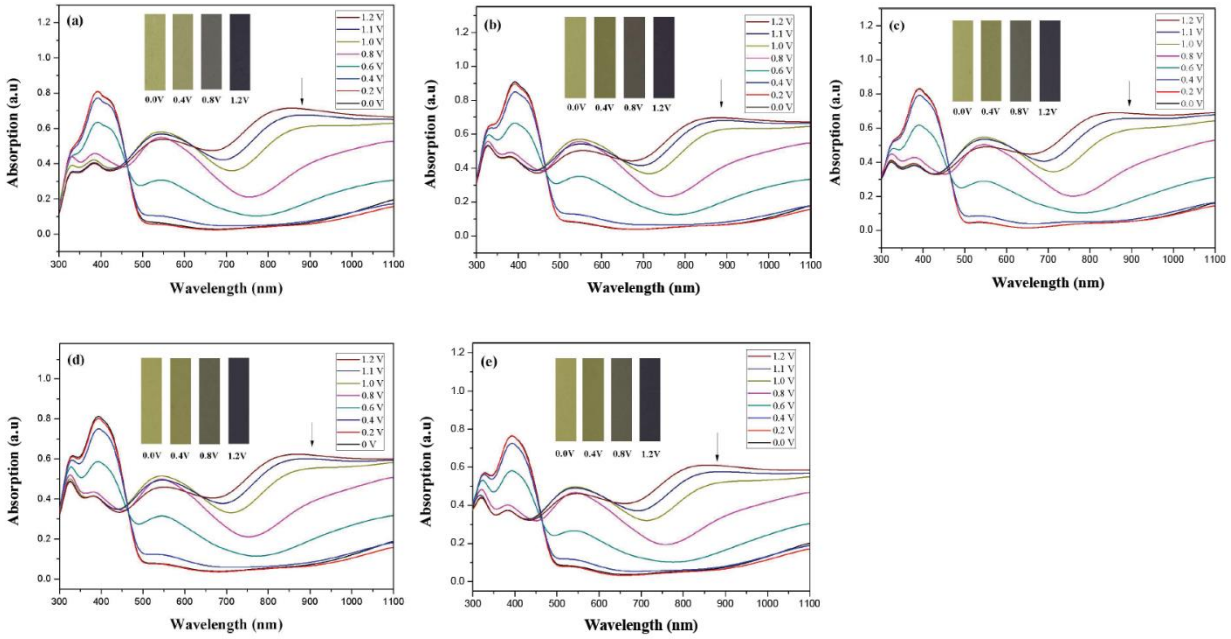

Figure 5. UV-Visible spectra of (**a**) PDTC, (**b**) P(DTC-*co*-BTP), (**c**) P(DTC-*co*-BTP2), (**d**) P(DTC-*co*-TF), and (**e**) P(DTC-*co*-TF2) in 0.2 M $LiClO_4$/ACN solution.

PDTC displays four types of colors from neutral to oxidation state; the color of PDTC is light yellow at 0.0 V, mustard yellow at 0.4 V, gray at 0.8 V, and dark gray at 1.2 V. The 2,2′-bithiophene- and 2-(2-thienyl)furan-based copolymers show different electrochromic properties with PDTC homopolymer. The colors of P(DTC-*co*-BTP) electrode are light yellow, yellowish-green, gray, and dark gray at 0.0, 0.4, 0.8, and 1.2 V, respectively, whereas P(DTC-*co*-BTP2) is dark yellow, khaki, gray, and dark gray at 0.0, 0.4, 0.8 V, and 1.2 V, respectively. For 2-(2-thienyl)furan-based copolymers, P(DTC-*co*-TF) is mustard yellow, khaki, grey, and dark grey at 0.0, 0.4, 0.8, and 1.2 V, respectively, P(DTC-*co*-TF2) is dark yellow, yellowish-green, gunmetal gray, and dark gray at 0.0, 0.4, 0.8, and 1.2 V, respectively. The colorimetric values, CIE chromaticity values, and charts of PDTC, P(DTC-*co*-BTP), P(DTC-*co*-BTP2), P(DTC-*co*-TF), and P(DTC-*co*-TF2) at 0.0—1.0 V are summarized in Table 2.

Table 2. Colorimetric values (L^*, a^*, and b^*), CIE chromaticity values (x, y), and CIE diagrams of (a) PDTC, (b) P(DTC-*co*-BTP), (c) P(DTC-*co*-BTP2), (d) P(DTC-*co*-TF), and (e) P(DTC-*co*-TF2) at various applied potentials.

Films	Potential (V)	L^*	a^*	b^*	x	y	Diagrams
(a)	0.0	70.45	−3.23	7.29	0.3235	0.3493	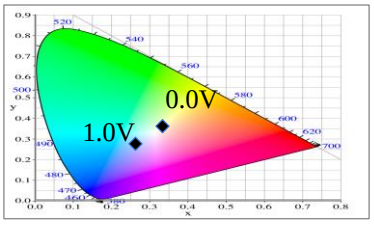
	0.4	67.3	−1.07	2.08	0.3157	0.3351	
	0.6	62.34	1.36	−5.18	0.3024	0.3144	
	0.8	55.89	−0.11	−13.45	0.2766	0.2913	
	1.0	52.01	−1.19	−17.14	0.2624	0.2794	
(b)	0.0	75.43	−2.85	11.33	0.3321	0.3571	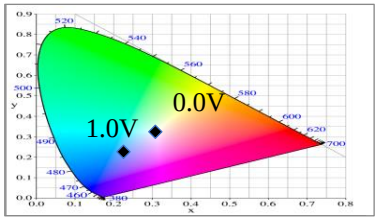
	0.4	72.02	−0.36	5.82	0.325	0.3429	
	0.6	66.68	2.7	−2.94	0.3106	0.3195	
	0.8	60.53	2.92	−12.11	0.2876	0.2947	
	1.0	54.06	1.08	−19.74	0.2614	0.2721	
(c)	0.0	95.82	−13.98	44.81	0.3683	0.4233	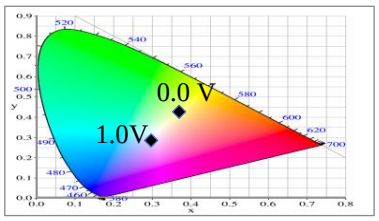
	0.4	92.85	−11.67	40.39	0.366	0.4154	
	0.6	78.43	−1.46	14.04	0.3393	0.3609	
	0.8	65.19	10.53	−12.6	0.3012	0.2899	
	1.0	62.19	11.62	−15.4	0.2957	0.2810	
(d)	0.0	93.35	−12.65	41.74	0.3665	0.4184	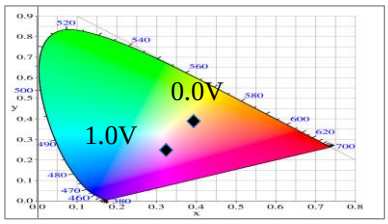
	0.4	90.01	−9.75	35.87	0.3627	0.4071	
	0.6	76.91	0.4	11.45	0.3375	0.354	
	0.8	65.57	10.39	−10.81	0.3053	0.2944	
	1.0	64.01	9.85	−11.98	0.3013	0.2914	
(e)	0.0	93.22	−11.1	39.37	0.3651	0.4126	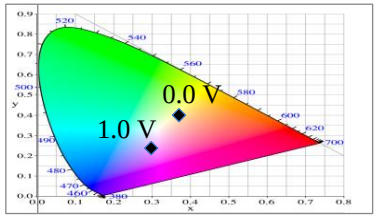
	0.4	90.72	−8.62	34.39	0.3616	0.4027	
	0.6	80.06	−0.69	14.72	0.3415	0.3611	
	0.8	67.38	10.15	−10.48	0.3059	0.296	
	1.0	65.00	10.16	−12.55	0.3006	0.2902	

3.3. Electrochromic Switching of Anodic Polymers

Figure 6 shows the transmittance-time plots of PDTC, P(DTC-*co*-BTP), P(DTC-*co*-BTP2), P(DTC-*co*-TF), and P(DTC-*co*-TF2) membranes caused by potential stepping between reduced and oxidized states. The residence time is 5 s. The ΔT of PDTC, P(DTC-*co*-BTP), P(DTC-*co*-BTP2), P(DTC-*co*-TF), and P(DTC-*co*-TF2) were 37.9% at 860 nm, 61.6% at 875 nm, 68.4% at 855 nm, 67.3% at 870 nm, and 56.1% at 855 nm, respectively (Table 3). The ΔT of 2,2′-bithiophene- and 2-(2-thienyl)furan-based copolymers (P(DTC-*co*-BTP), P(DTC-*co*-BTP2), P(DTC-*co*-TF), and P(DTC-*co*-TF2)) were higher than that of PDTC in 0.2 M $LiClO_4$/ACN, inferring that copolymers containing 2,2′-bithiophene or 2-(2-thienyl)furan groups increased ΔT significantly. Moreover, the ΔT of P(DTC-*co*-BTP2) was higher than those reported for P(PtCz-*co*-BTP2) [35], PITID-2 [36], P(HoT-BSe-OF) [37], PDTCZ-2 [38], and PI-6D [39] (Table 4). The bleaching response time (τ_b) and coloring response time

(τ_c) needed to reach 90% of the maximum transmittance change were determined to be 0.9–3.1 s for these polymers. The coloration efficiency (η) is a significant factor for effective utilization of polymers in electrochromic devices and it can be obtained using the equation below [40]:

$$\eta = \frac{\Delta OD}{Q_d} \quad (1)$$

where ΔOD and Q_d represent the change of optical density and the injected charges divided by active electrode area, respectively. As listed in Table 3, the η of PDTC, P(DTC-*co*-BTP), P(DTC-*co*-BTP2), P(DTC-*co*-TF), and P(DTC-*co*-TF2) were 125.8 cm^2 C^{-1} at 860 nm, 141.5 cm^2 C^{-1} at 875 nm, 159.4 cm^2 C^{-1} at 855 nm, 161.6 cm^2 C^{-1} at 870 nm, and 152.9 cm^2 C^{-1} at 855 nm, respectively. P(DTC-*co*-BTP2) shows higher η than that of P(HoT-BSe-OF) [37]. However, P(DTC-*co*-BTP2) shows a lower η than those of PITID-2 [36], PDTCZ-2 [38], and PI-6D [39] (Table 4).

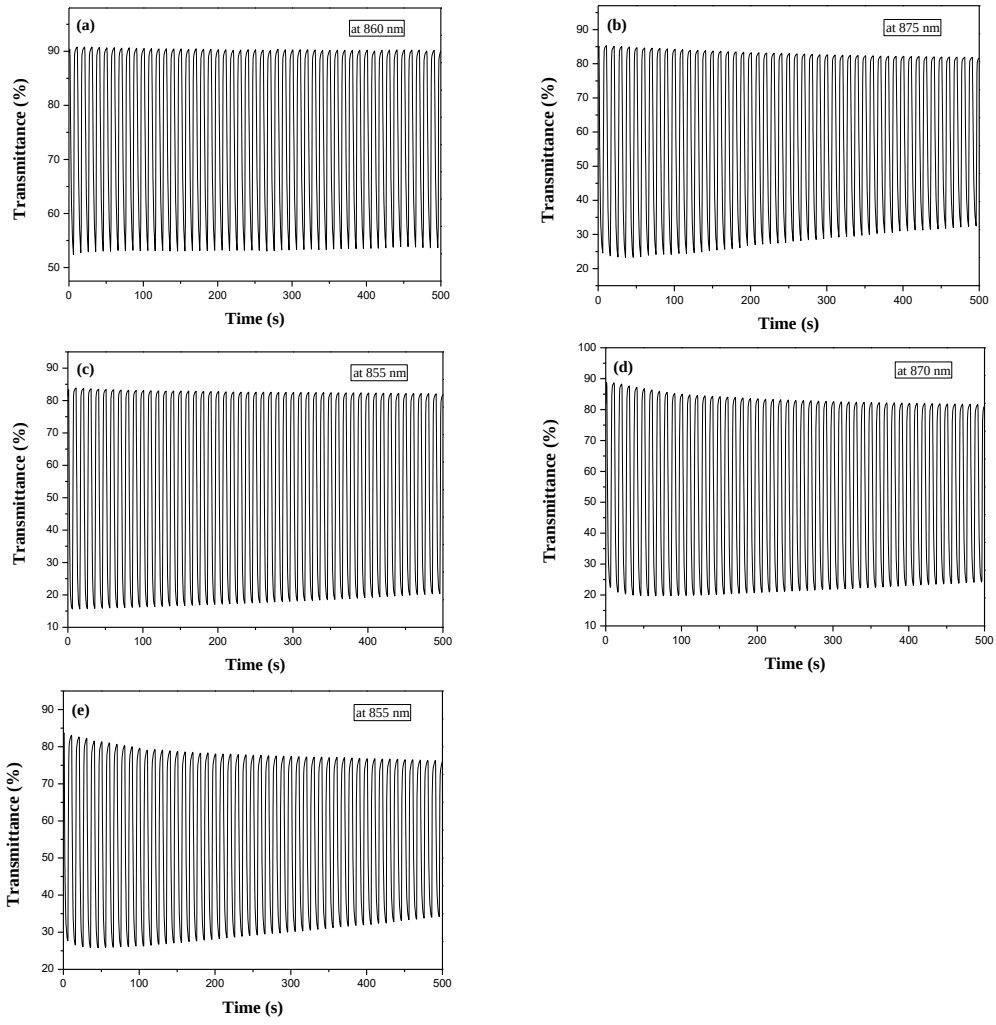

Figure 6. Optical contrast of (**a**) PDTC, (**b**) P(DTC-*co*-BTP), (**c**) P(DTC-*co*-BTP2), (**d**) P(DTC-*co*-TF), and (**e**) P(DTC-*co*-TF2) in 0.2 M $LiClO_4$/ACN solution with a residence time of 5 s.

Table 3. Optical properties of electrodes.

Electrodes	λ (nm)	T_{ox}	T_{red}	ΔT	ΔOD	Q_d (mC cm^{-2})	η (cm^2 C^{-1})	τ_c (s)	τ_b (s)
PDTC	860	52.8	90.7	37.9	0.24	1.87	125.8	3.1	1.2
	550	31.9	68.4	36.5	0.33	1.85	178.4	0.9	1.9
P(DTC-*co*-BTP)	875	23.6	85.2	61.6	0.56	3.94	141.5	3.1	1
	550	21.9	62.1	40.2	0.45	3.41	131.9	1.4	1.7
P(DTC-*co*-BTP2)	855	15.5	83.9	68.4	0.73	4.6	159.4	1.9	1
	550	23.7	65.6	41.9	0.44	3.36	130.9	1.3	1.9
P(DTC-*co*-TF)	870	21.3	88.6	67.3	0.62	3.83	161.6	3.4	1.8
	550	25.8	59.8	34	0.36	3.65	98.6	1.3	1.8
P(DTC-*co*-TF2)	855	26.8	82.9	56.1	0.49	3.21	152.9	3.1	1.2
	550	27.2	57.9	30.7	0.33	3.7	89.2	1.4	1.6

Table 4. Transmittance changes and coloration efficiencies of polymer films and ECDs.

Polymer Films or ECD Configurations	λ (nm)	ΔT (%)	η (cm^2 C^{-1})	References
P(PtCz-*co*-BTP2)	565	34	-	[35]
PITID-2	675	18	172	[36]
P(HoT-BSe-OF)	860	29	142	[37]
PDTCZ-2	898	30.7	169	[38]
PI-6D	568	57	250	[39]
P(DTC-*co*-BTP2)	855	68.4	159.4	This work
PETI/PEDOT	600	32	290	[41]
P(PS-Carb)/PEDOT	640	38	-	[26]
P(BCO)/PEDOT	620	35	-	[42]
P(DiCP-*co*-CPDTK)/PEDOT-PSS	635	38.2	633.8	[43]
P(DTC-*co*-TF)/PEDOT-PSS	627	43.4	496.0	This work

3.4. Spectroelectrochemical Properties of ECDs

Figure 7 showed the absorption spectra of PDTC/PEDOT-PSS, P(DTC-*co*-BTP)/PEDOT-PSS, P(DTC-*co*-BTP2)/PEDOT-PSS, P(DTC-*co*-TF)/PEDOT-PSS, and P(DTC-*co*-TF2)/PEDOT-PSS ECDs at assorted potentials. The five ECDs showed distinct UV-Visible bands *at* ca. 400 nm at around −0.5 V, which could be ascribed to the UV-Visible bands of PDTC, P(DTC-*co*-BTP), P(DTC-*co*-BTP2), P(DTC-*co*-TF), and P(DTC-*co*-TF2) at low potential zone. The UV-Visible bands of PDTC, P(DTC-*co*-BTP), P(DTC-*co*-BTP2), P(DTC-*co*-TF), and P(DTC-*co*-TF2) bleached with increasing potentials, and new visible peaks appeared bit by bit at 627–630 nm. This could be assigned to the reduction of PEDOT-PSS bit by bit. The colors of PDTC/PEDOT-PSS ECD are gray, dark gray, and *navy blue* at −0.5, 0.8, and 2.0 V, respectively. P(DTC-*co*-BTP)/PEDOT-PSS ECD is bright gray, dark gray, and deep blue at −0.5, 0.6, and 2.0 V, respectively. P(DTC-*co*-BTP2)/PEDOT-PSS ECD is bright gray, gunmetal grey, and berlin blue at −0.5, 0.8, and 2.0 V, respectively. P(DTC-*co*-TF)/PEDOT-PSS ECD is bright gray, iron grey, and sapphire at −0.5, 0.8, and 2.0 V, respectively. P(DTC-*co*-TF2)/PEDOT-PSS ECD is bright gray, gunmetal grey, and berlin blue at −0.5, 0.8, and 2.0 V, respectively. The photos, L^*, a^*, b^*, x, y, and CIE diagrams of PDTC/PEDOT-PSS, P(DTC-*co*-BTP)/PEDOT-PSS, P(DTC-*co*-BTP2)/PEDOT-PSS, P(DTC-*co*-TF)/PEDOT-PSS, and P(DTC-*co*-TF2)/PEDOT-PSS ECDs at different potentials are summarized in Table 5.

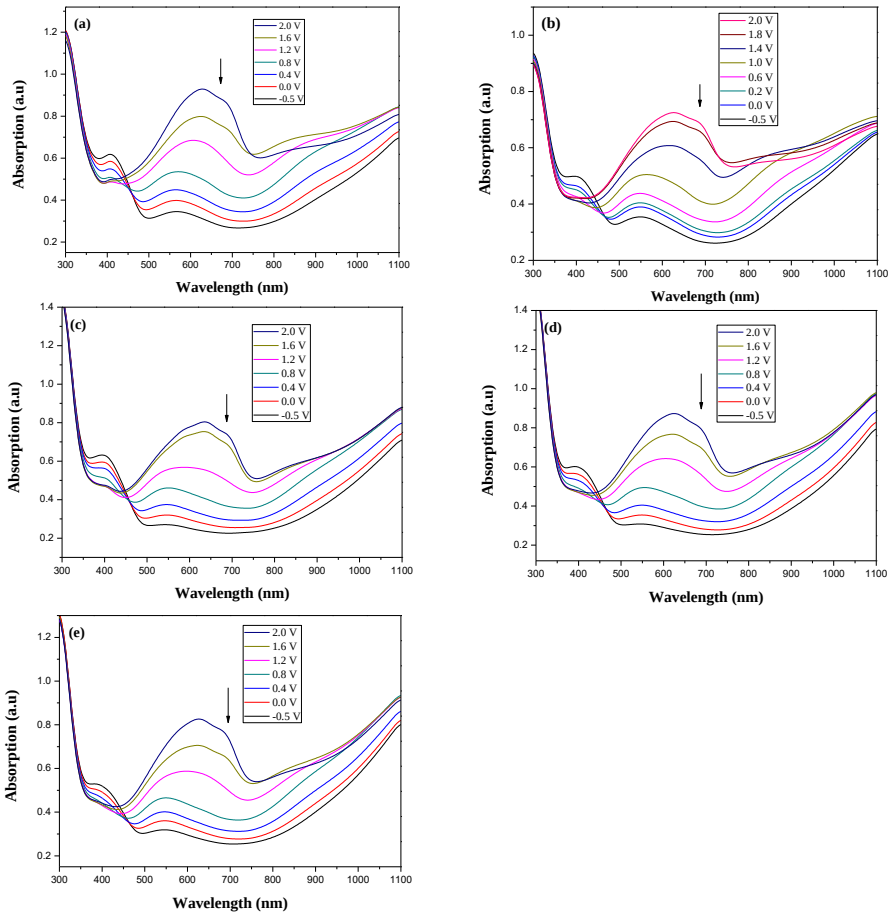

Figure 7. UV-Visible spectra of (**a**) PDTC/PEDOT-PSS, (**b**) P(DTC-*co*-BTP)/PEDOT-PSS, (**c**) P(DTC-*co*-BTP2)/PEDOT-PSS, (**d**) P(DTC-*co*-TF)/PEDOT-PSS, and (**e**) P(DTC-*co*-TF2)/PEDOT-PSS ECDs.

Table 5. Electrochromic photographs, colorimetric values (*L**, *a**, and b*) and CIE chromaticity values (*x*, *y*) of (a) PDTC/PEDOT-PSS, (b) P(DTC-*co*-BTP)/PEDOT-PSS, (c) P(DTC-*co*-BTP2)/PEDOT-PSS, (d) P(DTC-*co*-TF)/PEDOT-PSS, and (e) P(DTC-*co*-TF2)/PEDOT-PSS ECDs at various potentials.

ECDs	Potential (V)	Photographs	*L**	*a**	*b**	*x*	*y*	Diagrams
(a)	−0.5		73.76	−5.48	13.00	0.3314	0.3640	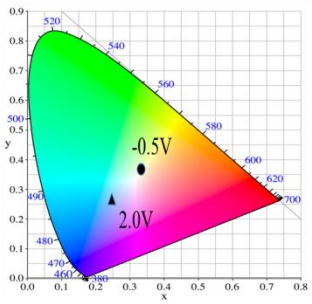
	0.0		70.45	−3.23	7.29	0.3235	0.3493	
	0.8		62.34	1.36	−5.18	0.3024	0.3144	
	1.2		55.89	−0.11	−13.45	0.2766	0.2913	
	1.6		52.01	−1.19	−17.14	0.2624	0.2794	
	2.0		48.40	−2.02	−21.74	0.2453	0.2638	
(b)	−0.5		73.29	−0.24	5.87	0.3251	0.3427	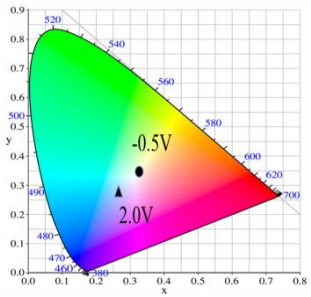
	0.0		70.17	2.45	−0.86	0.3180	0.3302	
	0.6		68.05	3.90	−4.33	0.3095	0.3154	
	1.4		59.39	1.73	−14.33	0.2795	0.2894	
	1.8		56.12	1.21	−17.49	0.2688	0.2795	
	2.0		55.16	0.83	−18.71	0.2643	0.2759	

Table 5. *Cont.*

ECDs	Potential (V)	Photographs	*L**	*a**	*b**	*x*	*y*	Diagrams
(c)	−0.5		78.63	−5.24	16.98	0.3390	0.3708	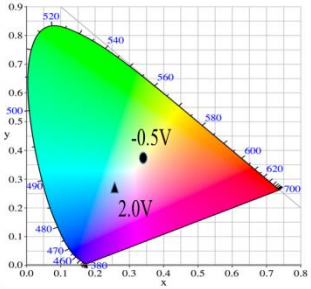
	0.0		75.43	−2.85	11.33	0.3321	0.3571	
	0.8		66.68	2.70	−2.94	0.3106	0.3195	
	1.2		60.53	2.92	−12.11	0.2876	0.2947	
	1.6		54.06	1.08	−19.74	0.2614	0.2721	
	2.0		52.64	0.45	−21.13	0.2555	0.2676	
(d)	−0.5		75.91	−4.19	14.22	0.3358	0.3647	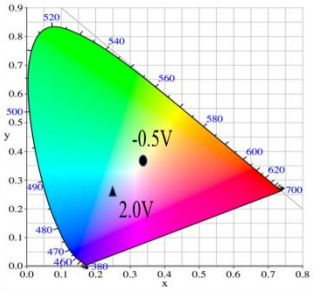
	0.0		73.10	−1.97	8.57	0.3281	0.3506	
	0.8		64.62	3.02	−5.16	0.3058	0.3135	
	1.2		57.52	1.82	−14.93	0.2772	0.2867	
	1.6		52.82	1.59	−19.79	0.2614	0.2706	
	2.0		49.75	0.79	−23.37	0.2477	0.2585	

Table 5. *Cont.*

ECDs	Potential (V)	Photographs	*L**	*a**	*b**	*x*	*y*	Diagrams
(e)	−0.5		73.57	−2.28	9.72	0.3300	0.3534	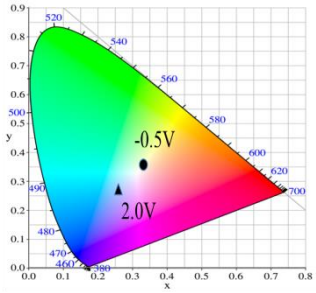
	0.0		71.28	−0.60	4.92	0.3227	0.3411	
	0.8		64.12	3.47	−6.6	0.3030	0.3094	
	1.2		58.17	2.20	−14.48	0.2794	0.288	
	1.6		54.37	1.44	−18.42	0.2657	0.2756	
	2.0		51.95	0.55	−20.23	0.2575	0.2694	

3.5. Colorless-to-Colorful Switching of ECDs

Figure 8 showed the potential stepping of PDTC/PEDOT-PSS, P(DTC-*co*-BTP)/PEDOT-PSS, P(DTC-*co*-BTP2)/PEDOT-PSS, P(DTC-*co*-TF)/PEDOT-PSS, and P(DTC-*co*-TF2)/PEDOT-PSS ECDs between colorless and colorful states with a residence time of 5 s. The ΔOD, ΔT, τ_b, and τ_c of PDTC/PEDOT-PSS, P(DTC-*co*-BTP)/PEDOT-PSS, P(DTC-*co*-BTP2)/PEDOT-PSS, P(DTC-*co*-TF)/PEDOT-PSS, and P(DTC-*co*-TF2)/PEDOT-PSS ECDs are displayed in Table 6. The ΔT_{max} of PDTC/PEDOT-PSS, P(DTC-*co*-BTP)/PEDOT-PSS, P(DTC-*co*-BTP2)/PEDOT-PSS, P(DTC-*co*-TF)/PEDOT-PSS, and P(DTC-*co*-TF2)/PEDOT-PSS ECDs are 34.3% at 630 nm, 38.7% at 630 nm, 41.6% at 630 nm, 43.4% at 627 nm, and 41.1% at 627 nm, respectively. P(DTC-*co*-TF)/PEDOT-PSS ECD showed the highest ΔT_{max}, and P(DTC-*co*-BTP)/PEDOT-PSS, P(DTC-*co*-BTP2)/PEDOT-PSS, P(DTC-*co*-TF)/PEDOT-PSS, and P(DTC-*co*-TF2)/PEDOT-PSS ECDs showed higher ΔT_{max} than that of PDTC/PEDOT-PSS ECD. This implies that the employment of copolymers (P(DTC-*co*-BTP), P(DTC-*co*-BTP2), P(DTC-*co*-TF), and P(DTC-*co*-TF2)) as the anodic layers results in a higher ΔT_{max} at ca. 627 nm than that of homopolymers (PDTCs). Table 4 lists ΔT's comparisons of P(DTC-*co*-TF)/PEDOT-PSS ECD with reported ECDs, showing that P(DTC-*co*-2BTP)/PEDOT-PSS ECD displays a higher ΔT than those reported for PETI/PEDOT [41], P(PS-Carb)/PEDOT [26], P(BCO)/PEDOT [42], and P(DiCP-*co*-CPDTK)/PEDOT-PSS ECDs [43].

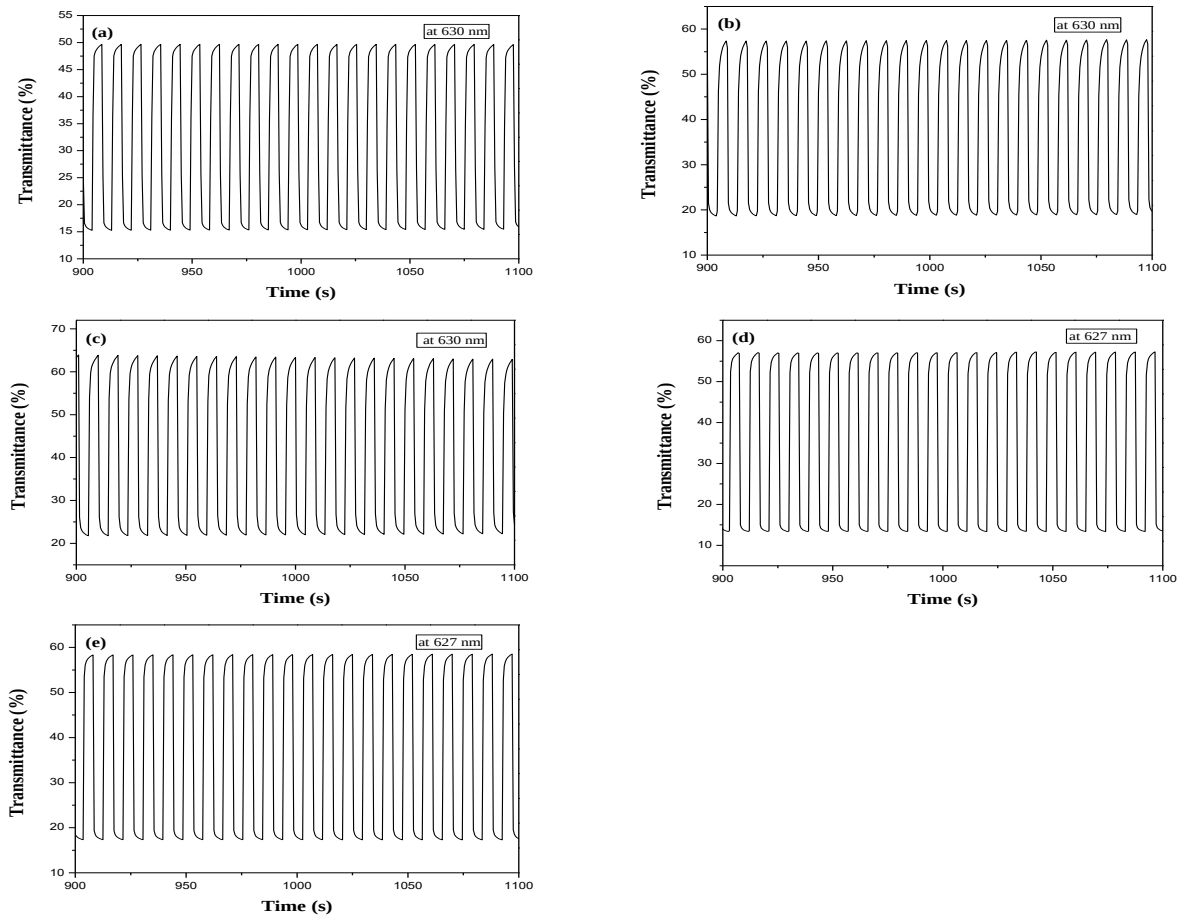

Figure 8. Optical contrast of (**a**) PDTC/PEDOT-PSS, (**b**) P(DTC-*co*-BTP)/PEDOT-PSS, (**c**) P(DTC-*co*-BTP2)/PEDOT-PSS, (**d**) P(DTC-*co*-TF)/PEDOT-PSS, and (**e**) P(DTC-*co*-TF2)/PEDOT-PSS ECDs with a residence time of 5 s.

Table 6. Optical properties of devices.

ECDs	T_{ox}	T_{red}	ΔT	ΔOD	Q_d (mC cm^{-2})	η (cm^2·C^{-1})	τ_c/s	τ_b/s
PDTC/PEDOT-PSS (630 nm)	15.4	49.7	34.3	0.509	1.21	420.7	0.9	0.7
P(DTC-*co*-BTP)/PEDOT-PSS (630 nm)	18.6	57.3	38.7	0.489	0.91	537.4	0.6	0.4
P(DTC-*co*-BTP2)/PEDOT-PSS (630 nm)	21.9	63.5	41.6	0.462	1.16	398.3	0.9	0.5
P(DTC-*co*-TF)/PEDOT-PSS (627 nm)	13.5	56.9	43.4	0.625	1.26	496	0.6	0.3
P(DTC-*co*-TF2)/PEDOT-PSS (627 nm)	17.3	58.4	41.1	0.528	1.03	512.6	0.5	0.4

The τ_b and τ_c of PDTC/PEDOT-PSS, P(DTC-*co*-BTP)/PEDOT-PSS, P(DTC-*co*-BTP2)/PEDOT-PSS, P(DTC-*co*-TF)/PEDOT-PSS, and P(DTC-*co*-TF2)/PEDOT-PSS ECDs in Table 6 are in the range of 0.3–0.9 s. τ_b and τ_c of five ECDs were shorter than their corresponding anodes in 0.2 M $LiClO_4$/ACN, revealing the ECDs switched color quicker than the anodes in 0.2 M $LiClO_4$/ACN from the colored to the bleached state [44].

The η of PDTC/PEDOT-PSS, P(DTC-*co*-BTP)/PEDOT-PSS, P(DTC-*co*-BTP2)/PEDOT-PSS, P(DTC-*co*-TF)/PEDOT-PSS, and P(DTC-*co*-TF2)/PEDOT-PSS ECDs are 420.7 cm^2 C^{-1} at 630 nm, 537.4 cm^2 C^{-1} at 630 nm, 398.3 cm^2 C^{-1} at 630 nm, 496.0 cm^2 C^{-1} at 627 nm, and 512.6 cm^2 C^{-1} at 627 nm, respectively. Among these ECDs, P(DTC-*co*-BTP) with a feed molar ratio of DTC/BTP = 1/1 displays the highest η. Table 4 displays η's comparisons of P(DTC-*co*-TF)/PEDOT-PSS ECD with reported ECDs, while P(DTC-*co*-TF)/PEDOT-PSS ECD shows a greater η than that reported for PETI/PEDOT ECD [41]. However, P(DTC-*co*-TF)/PEDOT-PSS ECD displays a lower η than that reported for P(DiCP-*co*-CPDTK)/PEDOT-PSS ECD [43].

3.6. Optical Memory Influences of ECDs

The optical memory influences of PDTC/PEDOT-PSS, P(DTC-co-BTP)/PEDOT-PSS, P(DTC-co-BTP2)/PEDOT-PSS, P(DTC-co-TF)/PEDOT-PSS, and P(DTC-co-TF2)/PEDOT-PSS ECDs were monitored in the colored and bleached states by exerting the voltage for 1 sec for each 100 sec interval. Figure 9 displayed that the transmittances of PDTC/PEDOT-PSS, P(DTC-co-BTP)/PEDOT-PSS, P(DTC-co-BTP2)/PEDOT-PSS, P(DTC-co-TF)/PEDOT-PSS, and P(DTC-co-TF2)/PEDOT-PSS ECDs experienced almost no change in the bleached state. On the other hand, the transmittance changes of PDTC/PEDOT-PSS, P(DTC-co-BTP)/PEDOT-PSS, P(DTC-co-BTP2)/PEDOT-PSS, P(DTC-co-TF)/PEDOT-PSS, and P(DTC-co-TF2)/PEDOT-PSS ECDs in the colored state were less electrochemically stable than those in the bleached state. However, the change of transmittance for ECDs in the colored states was less than 4.3%. P(DTC-co-TF2)/PEDOT-PSS ECD showed the lowest transmittance change (2.9%) in the colored state and P(DTC-co-BTP2)/PEDOT-PSS ECD showed the lowest transmittance change (0.2%) in the bleached state. Considering the aforementioned results, P(DTC-co-BTP)/PEDOT-PSS, P(DTC-co-BTP2)/PEDOT-PSS, P(DTC-co-TF)/PEDOT-PSS, and P(DTC-co-TF2)/PEDOT-PSS ECDs display acceptable optical memory.

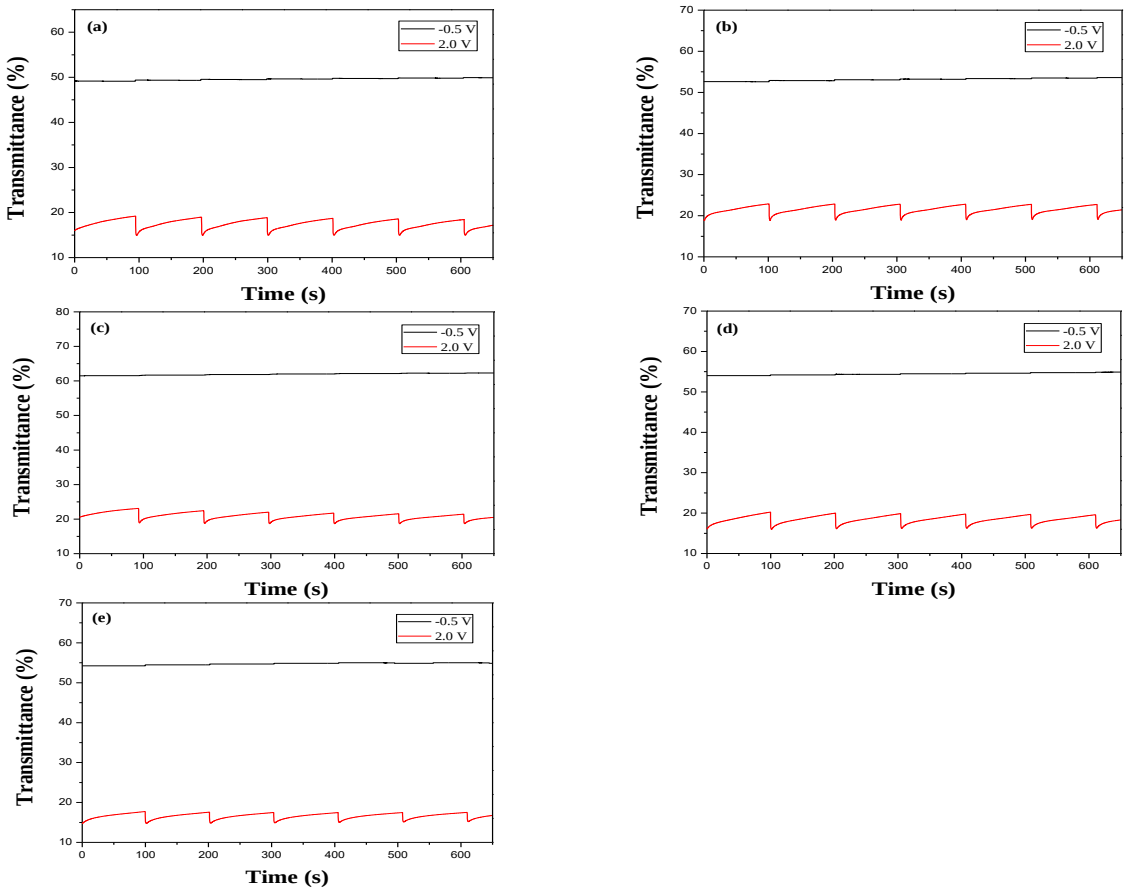

Figure 9. Open circuit stability of (**a**) PDTC/PEDOT-PSS, (**b**) P(DTC-*co*-BTP)/PEDOT-PSS, (**c**) P(DTC-*co*-BTP2)/PEDOT-PSS, (**d**) P(DTC-*co*-TF)/PEDOT-PSS, and (**e**) P(DTC-*co*-TF2)/PEDOT-PSS ECDs.

3.7. Redox Stability of ECDs

The long-term cycling stability measurement of PDTC/PEDOT-PSS, P(DTC-*co*-BTP)/PEDOT-PSS, P(DTC-*co*-BTP2)/PEDOT-PSS, P(DTC-*co*-TF)/PEDOT-PSS, and P(DTC-*co*-TF2)/PEDOT-PSS ECDs was carried out using CV at the first, 500th and 1000th cycles [45]. From the inspection of redox ability in Figure 10, 90.3%, 87.6%, 85.1%, 91.5%, and 89.7% of electroactivity are conserved at the 500th cycle, and 86.7%, 74.4%, 72.1%, 83.7%, and 84.6% of electroactivity are conserved at the 1000th cycle for PDTC/PEDOT-PSS, P(DTC-*co*-BTP)/PEDOT-PSS, P(DTC-*co*-BTP2)/PEDOT-PSS, P(DTC-*co*-TF)/PEDOT-PSS, and P(DTC-*co*-TF2)/PEDOT-PSS ECDs, respectively. P(DTC-*co*-TF)/PEDOT-PSS and P(DTC-*co*-TF2)/ PEDOT-PSS ECDs showed better cycling stability than those of P(DTC-*co*-BTP)/PEDOT-PSS and P(DTC-*co*-BTP2)/PEDOT-PSS ECDs, displaying ECDs employed 2-(2-thienyl)furan-containing P(DTC-*co*-TF) (or P(DTC-*co*-TF2)) as anodic layer led to a better cycling stability than that of 2,2′-bithiophene-containing P(DTC-*co*-BTP) (or P(DTC-*co*-BTP2)).

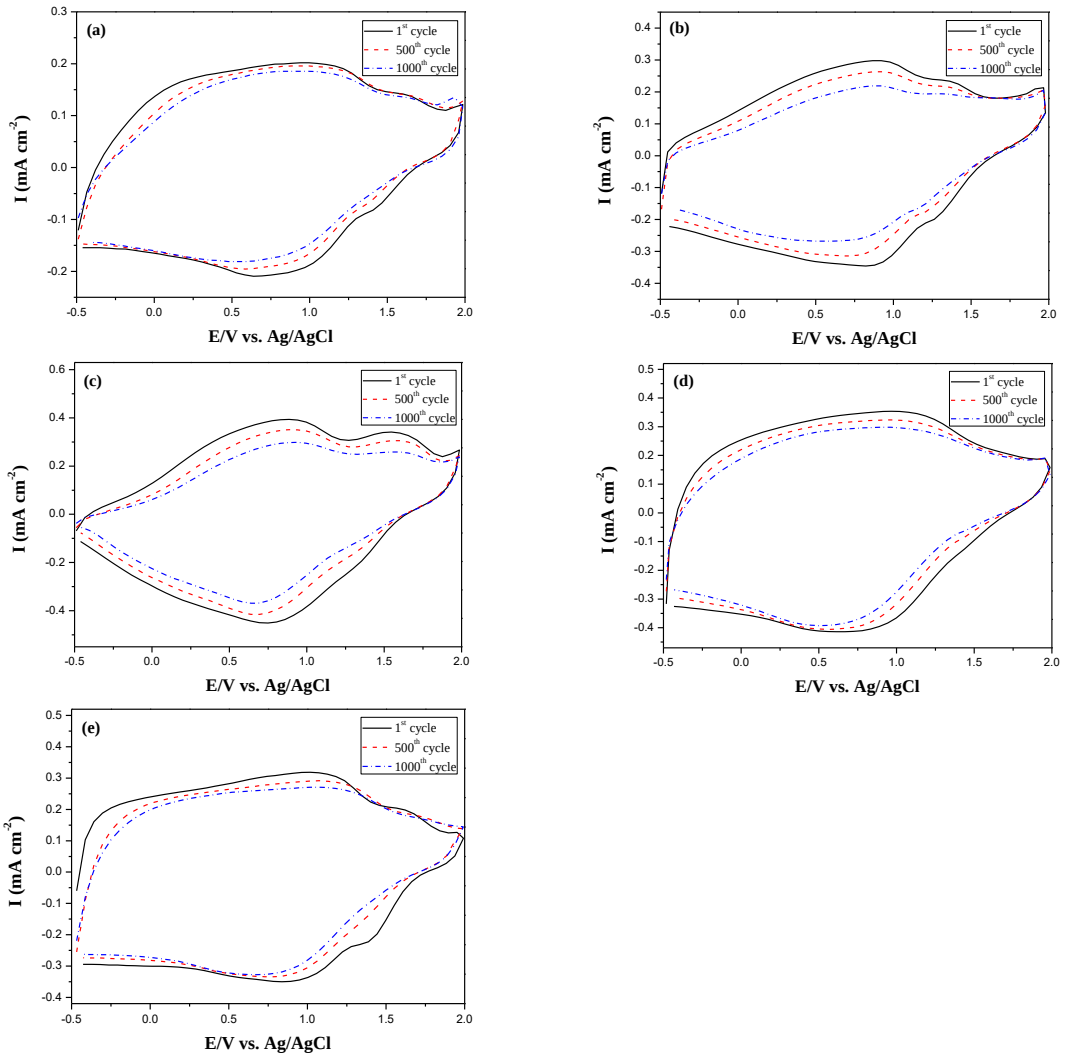

Figure 10. Cyclic voltammograms of (**a**) PDTC/PEDOT-PSS, (**b**) P(DTC-*co*-BTP)/PEDOT-PSS, (**c**) P(DTC-*co*-BTP2)/PEDOT-PSS, (**d**) P(DTC-*co*-TF)/PEDOT-PSS, and (**e**) P(DTC-*co*-TF2)/PEDOT-PSS devices with a scan rate of 500 mV s^{-1} between the 1st and 1000th cycles.

4. Conclusions

A series of ECDs' anodic materials (PDTC, P(DTC-*co*-BTP), P(DTC-*co*-BTP2), P(DTC-*co*-TF), and P(DTC-*co*-TF2)) were prepared electrochemically. The 2,2′-bithiophene- and 2-(2-thienyl)furan-based copolymers prepared with various monomer feed ratios displayed various colorimetry, spectroelectrochemical, and electrochromic switching performances. The colors of P(DTC-*co*-BTP) electrode are light yellow, yellowish-green, gray, and dark gray at 0.0, 0.4, 0.8, and 1.2 V, respectively. The ΔT of P(DTC-*co*-BTP), P(DTC-*co*-BTP2), P(DTC-*co*-TF), and P(DTC-*co*-TF2) in solutions were 61.6% at 875 nm, 68.4% at 855 nm, 67.3% at 870 nm, and 56.1% at 855 nm, respectively. Dual type polymer ECDs which consisted of 2,2′-bithiophene- and 2-(2-thienyl)furan-based anodically coloring membranes and a PEDOT-PSS cathodically coloring membrane were made. The transmittance changes of ECDs' optical memory test in the colored and bleached states were less than 4.3% and 0.4%, respectively. P(DTC-*co*-TF)/PEDOT-PSS ECD displays the highest ΔT (43.4% at 627 nm), whereas P(DTC-*co*-BTP)/PEDOT-PSS ECD shows the highest η (537.4 cm^2 C^{-1} at 630 nm). In view of the aforementioned performances, 2,2′-bithiophene- and 2-(2-thienyl)furan-based electrochromic membranes are suitable to apply in electrochromic goggles, e-skins, textiles, and wearable display devices.

Author Contributions: Conceptualization, C.-W.K.; formal analysis, C.-W.K. and S.-W.H.; investigation, C.-W.K. and S.-W.H.; resources, J.-K.C., J.-C.C. and P.-Y.L.; data curation, S.-W.H., J.-K.C., J.-C.C., P.-Y.L. and T.-Y.W.; writing—original draft preparation, C.-W.K. and T.-Y.W.; writing—review and editing, C.-W.K. and T.-Y.W.; project administration, C.-W.K. and S.-W.H.; funding acquisition, C.-W.K., T.-Y.W. and J.-K.C. All authors have read and agreed to the published version of the manuscript.

Funding: This research was funded by Ministry of Science and Technology of Republic of China, Grant No. 109-2221-E-992-006 and 108-2221-E-224-049-MY3.

Conflicts of Interest: The authors declare no conflict of interest.

References

1. Rosseinsky, D.R.; Mortimer, R.J. Electrochromic systems and the prospects for devices. *Adv. Mater.* **2001**, *13*, 783–793. [CrossRef]
2. Alesanco, Y.; Viñuales, A.; Rodriguez, J.; Tena-Zaera, R. All-in-one gel-based electrochromic devices: Strengths and recent developments. *Materials* **2018**, *11*, 414. [CrossRef]
3. Neo, W.T.; Ye, Q.; Chua, S.-J.; Xu, J. Conjugated polymer-based electrochromics: Materials, device fabrication and application prospects. *J. Mater. Chem. C* **2016**, *4*, 7364–7376. [CrossRef]
4. Mortimer, R.J.; Dyer, A.L.; Reynolds, J.R. Electrochromic organic and polymeric materials for display applications. *Displays* **2006**, *27*, 2–18. [CrossRef]
5. Herranz, D.; Coppola, R.E.; Escudero-Cid, R.; Ochoa-Romero, K.; D'Accorso, N.B.; Pérez-Flores, J.C.; Canales-Vázquez, J.; Palacio, C.; Abuin, G.C.; Ocón, P. Application of crosslinked polybenzimidazole-poly(vinyl benzyl chloride) anion exchange membranes in direct ethanol fuel cells. *Membranes* **2020**, *10*, 349. [CrossRef] [PubMed]
6. Dickinson, E.J.F.; Smith, G. Modelling the proton-conductive membrane in practical polymer electrolyte membrane fuel cell (PEMFC) simulation: A review. *Membranes* **2020**, *10*, 310. [CrossRef] [PubMed]
7. Navarrete, L.; Andrio, A.; Escolástico, S.; Moya, S.; Compañ, V.; Serra, J.M. Protonic conduction of partially-substituted CsH_2PO_4 and the applicability in electrochemical devices. *Membranes* **2019**, *9*, 49. [CrossRef] [PubMed]
8. Brza, M.; Aziz, S.B.; Saeed, S.R.; Hamsan, M.H.; Majid, S.R.; Abdulwahid, R.T.; Kadir, M.F.Z.; Abdullah, R.M. Energy storage behavior of lithium-ion conducting poly(vinyl alcohol) (PVA): Chitosan(CS)-based polymer blend electrolyte membranes: Preparation, equivalent circuit modeling, ion transport parameters, and dielectric properties. *Membranes* **2020**, *10*, 381. [CrossRef]
9. Lenar, N.; Paczosa-Bator, B.; Piech, R. Optimization of ruthenium dioxide solid contact in ion-selective electrodes. *Membranes* **2020**, *10*, 182. [CrossRef]
10. Mortimer, R.J. Electrochromic materials. *Annu. Rev. Mater. Res.* **2011**, *41*, 241–268. [CrossRef]
11. Guzela, M.; Karatasbz, E.; Ak, M. Synthesis and fluorescence properties of carbazole based asymmetric functionalized star shaped polymer. *J. Electrochem. Soc.* **2017**, *164*, H49–H55. [CrossRef]
12. Hsiao, S.H.; Wu, L.C. Fluorescent and electrochromic polymers from 2,8-di(carbazol-9-yl)dibenzothiophene and its S,S-dioxide derivative. *Dye. Pigment.* **2016**, *134*, 51–63. [CrossRef]
13. Kuo, C.W.; Wu, T.Y.; Huang, M.W. Electrochromic characterizations of copolymers based on 4,4′-bis(*N*-carbazolyl)-1,1′-biphenyl and indole-6-carboxylic acid and their applications in electrochromic devices. *J. Taiwan Inst. Chem. Eng.* **2016**, *68*, 481–488. [CrossRef]
14. Kuo, C.W.; Wu, T.L.; Lin, Y.C.; Chang, J.K.; Chen, H.R.; Wu, T.Y. Copolymers based on 1,3-bis(carbazol-9-yl)benzene and three 3,4-ethylenedioxythiophene derivatives as potential anodically coloring copolymers in high-contrast electrochromic devices. *Polymers* **2016**, *8*, 368. [CrossRef]
15. Liu, J.; Mi, S.; Xu, Z.; Wu, J.; Zheng, J.; Xu, C. Solution-processable thiophene-based electrochromic polymers bearing trifluoromethyl rather than long side chains. *Org. Electron.* **2016**, *37*, 169–177. [CrossRef]
16. Mo, D.; Zhou, W.; Ma, X.; Xu, J. Facile electrochemical polymerization of 2-(thiophen-2-yl)furan and the enhanced capacitance properties of its polymer in acetonitrile electrolyte containing boron trifluoride diethyl etherate. *Electrochim. Acta* **2015**, *155*, 29–37. [CrossRef]
17. Camurlu, P. Polypyrrole derivatives for electrochromic applications. *RSC Adv.* **2014**, *4*, 55832–55845. [CrossRef]
18. Wu, T.Y.; Li, W.B.; Kuo, C.W.; Chou, C.F.; Liao, J.W.; Chen, H.R.; Tseng, C.G. Study of poly(methyl methacrylate)-based gel electrolyte for electrochromic device. *Int. J. Electrochem. Sci.* **2013**, *8*, 10720–10732.
19. Hsiao, S.-H.; Lu, H.-Y. Electrosynthesis of aromatic poly(amide-amine) films from triphenylamine-based electroactive compounds for electrochromic applications. *Polymers* **2017**, *9*, 708. [CrossRef]
20. Lu, Q.; Cai, W.; Niu, H.; Wang, W.; Bai, X.; Hou, Y. Novel polyamides with 5H-dibenzo[b,f]azepin-5-yl-substituted triphenylamine: Synthesis and visible-NIR electrochromic properties. *Polymers* **2017**, *9*, 542. [CrossRef]
21. Hsiao, S.-H.; Liao, W.-K.; Liou, G.-S. Synthesis and electrochromism of highly organosoluble polyamides and polyimides with bulky trityl-substituted triphenylamine units. *Polymers* **2017**, *9*, 511. [CrossRef] [PubMed]
22. Kuo, C.-W.; Wu, T.-Y.; Fan, S.-C. Applications of poly(indole-6-carboxylic acid-*co*-2,2′-bithiophene) films in high-contrast electrochromic devices. *Coatings* **2018**, *8*, 102. [CrossRef]

23. Kuo, C.W.; Hsieh, T.H.; Hsieh, C.K.; Liao, J.W.; Wu, T.Y. Electrosynthesis and characterization of four electrochromic polymers based on carbazole and indole-6-carboxylic acid and their applications in high-contrast electrochromic devices. *J. Electrochem. Soc.* **2014**, *161*, D782–D790. [CrossRef]
24. Bekkar, F.; Bettahar, F.; Moreno, I.; Meghabar, R.; Hamadouche, M.; Hernáez, E.; Vilas-Vilela, J.L.; Ruiz-Rubio, L. Polycarbazole and its derivatives: Synthesis and applications. A review of the last 10 years. *Polymers* **2020**, *12*, 2227. [CrossRef] [PubMed]
25. Hsiao, S.H.; Hsueh, J.C. Electrochemical synthesis and electrochromic properties of new conjugated polycarbazoles from di(carbazol-9-yl)-substituted triphenylamine and *N*-phenylcarbazole derivatives. *J. Electroanal. Chem.* **2015**, *758*, 100–110. [CrossRef]
26. Oral, A.; Koyuncu, S.; Kaya, İ. Polystyrene functionalized carbazole and electrochromic device application. *Synth. Met.* **2009**, *159*, 1620–1627. [CrossRef]
27. Alkan, S.; Cutler, C.A.; Reynolds, J.R. High quality electrochromic polythiophenes via $BF_3{\cdot}Et_2O$ electropolymerization. *Adv. Funct. Mater.* **2003**, *13*, 331–336. [CrossRef]
28. Atılgan, N.; Cihaner, A.; Önal, A.M. Electrochromic performance and ion sensitivity of a terthienyl based fluorescent polymer. *React. Funct. Polym.* **2010**, *70*, 244–250. [CrossRef]
29. Kaur, S.; Findlay, N.J.; Kanibolotsky, A.L.; Elmasly, S.E.T.; Skabara, P.J.; Berridge, R.; Wilsonc, C.; Coles, S.J. Electrochromic properties of a poly(dithienylfuran) derivative featuring a redox-active dithiin unit. *Polym. Chem.* **2012**, *3*, 2277–2286. [CrossRef]
30. Zhen, S.J.; Lu, B.Y.; Xu, J.K.; Zhang, S.M.; Li, Y.Z. Poly(mono-, bi- or trifuran): Effect of oligomer chain length on the electropolymerization performances and polymer properties. *RSC Adv.* **2014**, *4*, 14001–14012. [CrossRef]
31. Su, Y.-S.; Wu, T.-Y. Three carbazole-based polymers as potential anodically coloring materials for high-contrast electrochromic devices. *Polymers* **2017**, *9*, 284. [CrossRef]
32. Kuo, C.W.; Chen, B.K.; Li, W.B.; Tseng, L.Y.; Wu, T.Y.; Tseng, C.G.; Chen, H.R.; Huang, Y.C. Effects of supporting electrolytes on spectroelectrochemical and electrochromic properties of polyaniline-poly(styrene sulfonic acid) and poly(ethylenedioxythiophene)-poly(styrene sulfonic acid)-based electrochromic device. *J. Chin. Chem. Soc.* **2014**, *61*, 563–570. [CrossRef]
33. Feng, F.; Kong, L.; Du, H.; Zhao, J.; Zhang, J. Donor-acceptor-type copolymers based on 3,4-propylenedioxy-thiophene and 5,6-difluorobenzotriazole: Synthesis and electrochromic properties. *Polymers* **2018**, *10*, 427. [CrossRef]
34. Kuo, C.W.; Lee, P.Y. Electrosynthesis of copolymers based on 1,3,5-tris(*N*-carbazolyl)benzene and 2,2′-bithiophene and their applications in electrochromic devices. *Polymers* **2017**, *9*, 518. [CrossRef] [PubMed]
35. Kalay, I.; Yiğit, D.; Güllü, M.; Depci, T.; Toppare, L.; Hacioglu, S.O. Enhancing electrochemical and electrochromic performances of carbazole comprising monomer via copolymerization with 3,4-ethylenedioxythiophene (EDOT). *Synth. Met.* **2020**, *267*, 116449. [CrossRef]
36. Zhang, Y.; Chen, S.; Zhang, Y.; Du, H.; Zhao, J. Design and characterization of new D–A Type electrochromic conjugated copolymers based on indolo [3,2-b]carbazole, isoindigo and thiophene units. *Polymers* **2019**, *110*, 1626. [CrossRef]
37. Xu, J.; Ji, Q.; Kong, L.; Du, H.; Ju, X.; Zhao, J. Soluble electrochromic polymers incorporating benzoselenadiazole and electron donor units (carbazole or fluorene): Synthesis and electronic-optical properties. *Polymers* **2018**, *10*, 450. [CrossRef] [PubMed]
38. Zhang, Y.; Kong, L.; Ju, X.; Du, H.; Zhao, J.; Xie, Y. Synthesis and characterization of novel donor–acceptor type neutral green electrochromic polymers containing an indolo[3,2-b]carbazole donor and diketopyrrolopyrrole acceptor. *RSC Adv.* **2018**, *8*, 21252. [CrossRef]
39. Zheng, R.; Huang, T.; Zhang, Z.; Sun, Z.; Niu, H.; Wang, C.; Wang, W. Novel polyimides containing flexible carbazole blocks with electrochromic and electrofluorescencechromic properties. *RSC Adv.* **2020**, *10*, 6992. [CrossRef]
40. Su, Y.S.; Chang, J.C.; Wu, T.Y. Applications of three dithienylpyrroles-based electrochromic polymers in high-contrast electrochromic devices. *Polymers* **2017**, *9*, 114. [CrossRef]
41. Yang, X.Y.; Liu, C.L.; Guo, J.B.; Wang, L.; Nie, G.M. A free-standing electrochromic material of poly(5,7-bis(2-(3,4-ethylenedioxy)thienyl)-indole) and its application in electrochromic device. *J. Polym. Sci. Part A Polym. Chem.* **2017**, *55*, 2356–2364. [CrossRef]
42. Udum, Y.A.; Hızlıateş, C.G.; Ergün, Y.; Toppare, L. Electrosynthesis and characterization of an electrochromic material containing biscarbazole–oxadiazole units and its application in an electrochromic device. *Thin Solid Films* **2015**, *595*, 61–67. [CrossRef]
43. Kuo, C.W.; Wu, B.W.; Chang, J.K.; Chang, J.C.; Lee, L.T.; Wu, T.Y.; Ho, T.H. Electrochromic devices based on poly(2,6-di(9Hcarbazol-9-yl)pyridine)-type polymer films and PEDOT-PSS. *Polymers* **2018**, *10*, 604. [CrossRef] [PubMed]
44. Kuo, C.-W.; Chang, J.-C.; Lee, P.-Y.; Wu, T.-Y.; Huang, Y.-C. Applications of electrochromic copolymers based on tris(4-carbazoyl-9-ylphenyl)amine and bithiophene derivatives in electrochromic devices. *Materials* **2018**, *11*, 1895. [CrossRef] [PubMed]
45. Kuo, C.W.; Chang, J.K.; Lin, Y.C.; Wu, T.Y.; Lee, P.Y.; Ho, T.H. Poly(tris(4-carbazoyl-9-ylphenyl)amine)/three poly(3,4-ethylenedioxythiophene) derivatives complementary high-contrast electrochromic devices. *Polymers* **2017**, *9*, 543. [CrossRef] [PubMed]